

An imprint of intrinsic quark–gluon correlations: a nonmonotonic feature in $e(x)$.

Chao Shi,^{1,*} Liming Lu,¹ Ian Cloët,^{2,†} Wenbao Jia,¹ and Peter Tandy^{3,‡}

¹*Department of Nuclear Science and Technology,
Nanjing University of Aeronautics and Astronautics, Nanjing 210016, China*

²*Physics Division, Argonne National Laboratory, Lemont, IL 60439, USA*

³*Center for Nuclear Research, Department of Physics, Kent State University, Kent OH 44242 USA*

We present the first rainbow–ladder Dyson–Schwinger equations study of the pion’s chiral-odd, twist-3 parton distribution $e_q(x)$. By deriving a novel Dyson–Schwinger equation for the pion’s quark–quark correlation matrix, we simultaneously extract from it both the unpolarized twist-2 parton distribution function $f_q(x)$ and the twist-3 distribution $e_q(x)$. Our results show that chiral symmetry strongly suppresses the twist-2 component of $e_q(x)$, leaving the genuine twist-3 quark–gluon component dominant and featuring a node. We therefore argue that the genuine twist-3 term can make a substantial contribution to hadronic $e(x)$, producing a nonmonotonic structure that is a clear imprint of intrinsic quark–gluon correlations. We point out that the existence of a hump-like feature is compatible with, although not uniquely indicated by, recent proton extractions and awaits more precise determination.

Introduction: Parton distribution functions (PDFs) encode the nonperturbative quark and gluon structure of hadrons and are probed in high-energy inclusive and semi-inclusive scattering processes. They comprise a variety of unpolarized and polarized distributions, with or without transverse-momentum dependence, and appear at different orders in the $1/Q$ expansion, where Q is the hard scale of the process. Leading contributions scale as $1/Q^0$ and originate from twist-2 QCD operators, while power-suppressed corrections ($1/Q, 1/Q^2$, etc.) arise from operators of higher twist. The unpolarized quark and gluon PDFs, $f(x)$ and $g(x)$, are twist-2 and have a clear single-particle probabilistic interpretation. In contrast, higher-twist distributions involve multiparton correlations, offering deeper insight into hadron structure but posing greater theoretical challenges [1, 2]. Upcoming measurements, including those at the planned Electron-Ion Collider, are expected to shed new light on these higher-twist effects [3, 4]. Herein we study the chiral-odd twist-3 unpolarized distribution $e_q(x)$ of the pion, aiming to illuminate the structure of twist-3 distributions in general. Possible extension to the nucleon $e_q(x)$ distribution is considered, for which preliminary data are already available.

The twist-3 PDF $e_q(x)$: The unpolarized twist-3 PDF $e_q(x)$ for quark flavor q in hadron h , in Minkowski metric, is defined as [1, 5]

$$e_q(x) = \frac{P \cdot n}{M_h} \int \frac{d\lambda}{4\pi} e^{ixP \cdot n\lambda} \langle P | \bar{\psi}_q(0) L_4 W[0, \lambda n] \psi_q(\lambda n) | P \rangle , \quad (1)$$

where $W[0, \lambda n]$ is the Wilson line gauge link. This Lorentz invariant form is facilitated by the light cone basis vector n , which in the target rest frame is $n = (1, -1, \vec{0})$, and thus $a \cdot n = a^+ = a^0 + a^3$ [1, 5]. This twist-3 PDF encodes novel features that are absent in twist-2 PDFs such

as the unpolarized quark PDF $f_q(x)$. The latter is given by replacing the unit matrix I_4 by $\gamma \cdot n$ and removing the prefactor $P \cdot n / M_h$. To separate the genuine twist-3 and twist-2 components of Eq. (1), an expansion of the non-local quark field current operator about its local limit ($\lambda = 0$) has been explored [2, 6] through use of the QCD equation of motion for the quark field. This leads to the gauge invariant decomposition [2, 6]

$$e_q(x) = \frac{\langle h | \bar{\psi}_q(0) \psi_q(0) | h \rangle}{2M_h} \delta(x) + e_q^{\text{mass}}(x) + e_q^{\text{tw3}}(x) , \quad (2)$$

in which the pure quark term $e_q^{\text{mass}}(x)$ is twist-2, while $e_q^{\text{tw3}}(x)$ is generated from quark–gluon correlations and is genuinely twist-3. Some exact features of the three terms have been derived [2] in terms of their Mellin moments $\langle x^m \rangle_e = \int dx x^m e(x)$ which produce

$$m = 0 \Rightarrow \langle x^0 \rangle_{e_q} = \frac{\sigma_q}{m_q} ; \quad \langle x^0 \rangle_{e_q^{\text{mass}}} = \langle x^0 \rangle_{e_q^{\text{tw3}}} = 0 , \quad (3)$$

and

$$m = 1 \Rightarrow \langle x \rangle_{e_q} = \langle x \rangle_{e_q^{\text{mass}}} = \frac{m_q}{M_h} ; \quad \langle x \rangle_{e_q^{\text{tw3}}} = 0 , \quad (4)$$

and

$$m \geq 2 \Rightarrow \langle x^m \rangle_{e_q^{\text{mass}}} = \frac{m_q}{M_h} \langle x^{m-1} \rangle_{f_q} ; \quad \langle x^m \rangle_{e_q^{\text{tw3}}} \neq 0 . \quad (5)$$

It is important to note that the m_q in the above exact results is the current quark mass. We use σ_q to denote the quark flavor q contribution to the hadron sigma term: $\sigma_u + \sigma_d$ gives σ_π for the nucleon, and σ_π for the π^+ .

Note that although the above is consistent with all moments of $x e_q^{\text{mass}}(x) = \frac{m_q}{M_h} f_q(x)$, the expression $\frac{m_q}{M_h} f_q(x) / x$ does not accurately account for $e_q^{\text{mass}}(x)$ itself, especially at small x , since Eq. (3) would not be satisfied. The low moment properties for the distribution $x e_q(x)$ [2] offer a strong hint at dominant features for light quarks: the $x e_q^{\text{mass}}(x)$ term should be a minor contribution due to

* cshi@nuua.edu.cn

† icloet@anl.gov

‡ tandy@kent.edu

the relatively small current quark mass; the remaining $xe_q^{\text{tw3}}(x)$ term integrates to zero, hence it likely changes sign with at least one node, assuming valence-quark dominance over antiquarks. These features are therefore expected to hold for the physical pion, a conclusion supported by our numerical results presented below.

The topic of how to separate the three contributions of Eq. (2) has attracted extensive discussion in theoretical analyses [7–9] and nonperturbative models [10–12]. Unfortunately, lattice QCD has not yet constrained $e_q^{\text{tw3}}(x)$ [8], and existing nucleon extractions of the total $e_q(x)$ from data carry large uncertainties [13, 14]. In this work we calculate the Mellin moments of the entire $e_q(x)$ of the pion using a nonperturbative framework based on the rainbow-ladder truncation of the Dyson–Schwinger equations of QCD. We use this DSE-RL approach to obtain the moments of the twist-2 term $xe_q^{\text{mass}}(x)$ and then identify the remaining genuine twist-3 term $xe_q^{\text{tw3}}(x)$. The calculation is performed in Euclidean space, where the formulation in terms of integral equations enables an effective resummation of infinite classes of diagrams for two- and three-point functions. The DSE-RL framework offers several key advantages for studying $e(x)$: (i) it retains explicit gluon degrees of freedom, (ii) it generates dynamical quark mass functions from current quark masses, and (iii) it preserves chiral symmetry, which could strongly influence $xe_q^{\text{mass}}(x)$ and thus the deduced $xe_q^{\text{tw3}}(x)$.

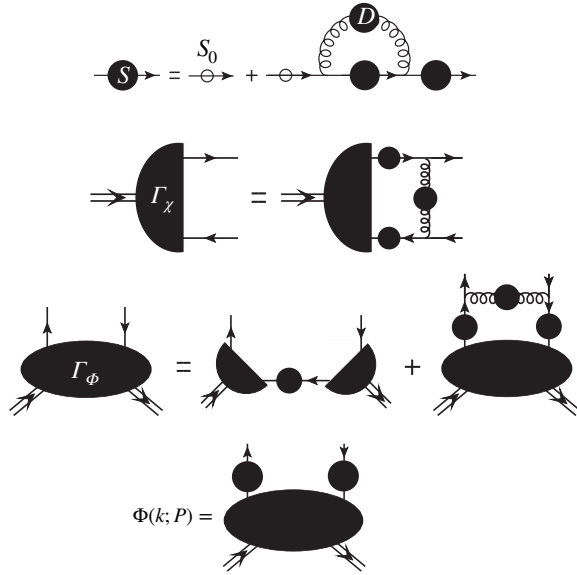


FIG. 1. The first three rows are the rainbow-ladder truncated DSEs for dressed quark propagator S , the amputated Bethe-Salpeter bound state vertex $\Gamma_\chi(k; P)$, and the amputated quark-quark correlation matrix $\Gamma_\Phi(k; P)$ respectively. The fourth row relates the unamputated quark-quark correlation matrix $\Phi(k; P)$ to $\Gamma_\Phi(k; P)$.

Pion's quark-quark correlation matrix and rainbow-ladder DSE approach: To facilitate a numerical momentum space DSE-RL treatment of several

different types of PDF for a hadron we omit the gauge link and recast Eq. (1) into the equivalent 2-step form [15, 16]

$$\Phi_{ij}(k, P) = \int d^4\xi e^{ik_\eta \cdot \xi} \langle P | \bar{\psi}_j(0) \psi_i(\xi) | P \rangle , \quad (6)$$

followed by

$$F(x) = \frac{1}{2} \int \frac{d^4k}{(2\pi)^4} \delta(k_\eta \cdot n - x P \cdot n) \text{Tr} [\Phi(k, P) \Gamma_F] . \quad (7)$$

Here $\Phi_{ij}(k, P)$ is the quark-quark correlator matrix for the hadron and $F(x)$ is the PDF associated with the choice of Dirac matrix Γ_F . The PDFs $f_q(x)$ and $e_q(x)$ follow from $\Phi_{ij}(k, P)$ with use of $\Gamma_F = \not{p}$ and $\Gamma_F = I_4 \frac{P \cdot n}{M_\pi}$ respectively. Note we have chosen $k_\eta \equiv k + \eta P$ as the momentum of the struck quark parton.

The rainbow-ladder truncation preserves the chiral symmetry of QCD and facilitates the associated consequences such as its dynamical breaking to generate constituent quark mass functions. It also implements color singlet vector current conservation and the partial conservation of the color singlet axial vector current. The DSE-RL approach to QCD consists of truncated equations of motion (EOM) for generalized Green functions $\langle \Omega | \hat{O}(\psi, \bar{\psi}, A) | \Omega \rangle$ [17, 18]. An overview of the QCD content appropriate to the present task is illustrated in Fig. 1. There row 1 displays the dressed quark propagator $S = \langle \Omega | \hat{T}\{\psi(x)\bar{\psi}(y)\} | \Omega \rangle$ as given by the rainbow-ladder integral equation. Row 2 displays the integral equation for the Bethe-Salpeter (BS) bound state amputated vertex $\langle \Omega | \hat{T}\{\psi(x)\bar{\psi}(y)\} | P \rangle$ for the pion. The 4-point function representing the amputated pion quark-quark correlation matrix Γ_Φ is depicted in row 3. The unamputated version Φ , defined in Eq. (6), is depicted in row 4. They are related by $\Phi = S \Gamma_\Phi S$.

Detailed momentum space representations within the DSE-RL truncation are as follows. The dressed quark propagator is obtained from

$$S(k)^{-1} = Z_2 (i \not{k} + Z_4 m_q(\mu)) + Z_2^2 \int_q^\Lambda g^2 D_{\mu\nu}(q) \frac{\lambda^a}{2} \gamma_\mu S(k-q) \frac{\lambda^a}{2} \gamma_\nu , \quad (8)$$

which is equivalent to the first row of Fig. 1, with the open circle S_0 denoting the bare quark propagator. Here \int_q^Λ represents $\int d^4q/(2\pi)^4$ with a smooth Poincaré invariant ultraviolet regularization at mass-scale Λ . The $m_q(\mu)$ is the current quark mass renormalized at scale μ . The Z_2 and Z_4 are the quark field and mass renormalization constants respectively. The factor Z_2^2 preserves multiplicative renormalizability in solutions of the DSE and BSE [19]. The $D_{\mu\nu}$ is in Landau gauge and it models a combination of quark-gluon vertex and gluon propagator [17, 18], with details specified later. The BS bound state vertex is

n	0	1	2	3	4	5	6	7	8
$\langle x^m \rangle_{f_q(x)}$	1.00	0.372	0.202	0.129	0.0910	0.0680	0.0531	0.0428	0.0358
$\langle x^m \rangle_{e_q(x)}$	6.45	0.113	0.303	0.278	0.231	0.191	0.159	0.134	0.115
$\langle x^m \rangle_{e_q^{\text{mass}}(x)}$	0	0.113	0.0419	0.0228	0.0146	0.0103	0.00773	0.00604	0.00488
$\langle x^m \rangle_{e_q^{\text{tw3}}(x)}$	0	0	0.261	0.255	0.216	0.181	0.151	0.128	0.110

TABLE I. Computed Mellin moments of unpolarized pion PDFs $f_q(x)$ for twist-2 and $e_q(x)$ for twist-3. Two components of $e_q(x)$ are shown and we note that $e_q^{\text{mass}}(x)$ is an estimated maximum as discussed in the text.

obtained via the integral equation

$$\Gamma_\chi(k; P) = -Z_2^2 \int_q^\Lambda g^2 D_{\mu\nu}(k-q) \gamma_\mu^a S(q_\eta) \Gamma_\chi(q; P) S(q_{\bar{\eta}}) \gamma_\nu^a, \quad (9)$$

with $\gamma_\mu^a \equiv \frac{\lambda^a}{2} \gamma_\mu$, and illustrated in the second row of Fig. 1. The quark momenta are $q_\eta = q + \eta P$ and $q_{\bar{\eta}} = q - (1 - \eta)P$, with $\eta = \frac{1}{2}$ used throughout this work.

The amputated pion quark-quark correlation matrix Γ_Φ is the 4-point function obtained via the integral equation

$$\Gamma_\Phi(k; P) = \Gamma_\chi(k; P) S(k_{\bar{\eta}}) \bar{\Gamma}_\chi(k; -P) - Z_2^2 \int_q^\Lambda g^2 D_{\mu\nu}(k-q) \gamma_\mu^a S(q_\eta) \Gamma_\Phi(q; P) S(q_{\bar{\eta}}) \gamma_\nu^a, \quad (10)$$

and illustrated in the third row of Fig. 1. The first term on the right hand side is the driving term and the second term incorporates all ladder gluon dressings. It is important to point out that this approach, centered around the collection of all gluon ladders into Γ_Φ , is quite different from DSE-RL approaches to PDFs that collect all such ladders to calculate a dressed quark vertex. This latter dressed quark vertex approach, e.g. Refs. [20, 21], has to be carried out separately for each different bare quark vertex Dirac matrix associated with the PDF of interest. In contrast, the ladder-summed quark-quark correlation matrix Γ_Φ depends only on the hadron; it can be used in Eq. (7) with a variety of bare quark vertices Γ_F to yield a variety of PDFs.

Numerical implementation: Calculations are facilitated by Euclidian metric¹. In this work we employ for $g^2 D_{\mu\nu}$ the infrared term of the Maris-Tandy kernel [22] as subsequently restructured [23]. Since the main features of parton distributions are dominated by soft infrared dynamics, we neglect the ultraviolet tail to facilitate this initial numerical exploration of $e_q(x)$ based on the dressed quark-quark correlator. Thus we use

$$g^2 D_{\mu\nu}(k) = \frac{8\pi^2}{\omega^4} D e^{-k^2/\omega^2} \left(\delta_{\mu\nu} - \frac{k_\mu k_\nu}{k^2} \right). \quad (11)$$

Given this super-renormalizable form, the explicit scale dependence of m_q, Z_2, Z_4 is unnecessary, and thus $Z_2 =$

¹ In Euclidean metric we employ $a_4 = ia^0$ for any space-time vector, including n , while $\{\gamma_\alpha, \gamma_\beta\} = 2\delta_{\alpha\beta}$ with $\gamma_4 = \gamma^0$. Hence $\not{a} \rightarrow -i\not{a}$ while $a \cdot b \rightarrow -a \cdot b$.

$Z_4 = 1$. Model parameters involved are the current quark mass $m_{u/d} = 5.5$ MeV, $\omega = 0.5$ GeV and $D\omega = (0.82\text{GeV})^3$, which reproduce the physical pion mass and decay constant as well as the ρ meson and nucleon properties [23–25].

The general Dirac structure of the relevant functions is as follows: $S(k)^{-1} = i\not{k} A(k^2) + B(k^2)$, while the meson bound state vertex Γ_χ from Eq. (9) has the form

$$\Gamma_\chi(k; P) = \gamma^5 \left(\sum_{i=1}^4 T_i \mathcal{F}_{\chi,i}(k^2, k \cdot P, P^2) \right), \quad (12)$$

and the amputated pion quark-quark correlation matrix Γ_Φ from Eq. (10) has the form

$$\Gamma_\Phi(k; P) = \sum_{i=1}^4 T_i \mathcal{F}_{\Phi,i}(k^2, k \cdot P, P^2). \quad (13)$$

We have used Dirac matrix covariants $T = \{I_4, \not{P}, \not{k}, [\not{k}, \not{P}]\}$ consistent with parity, time reversal and charge conjugation [26]. The A, B functions as well as the four amplitudes $\mathcal{F}_{\chi/\Phi} = \{E_{\chi/\Phi}, F_{\chi/\Phi}, G_{\chi/\Phi}, H_{\chi/\Phi}\}$ are Lorentz scalars. They can be obtained numerically via a medium sized computer cluster by combining Eqs. (8–13) to produce results for the correlator $\Phi(k; P) = S(k_\eta) \Gamma_\Phi(k; P) S(k_\eta)$.

Pion twist-2 and twist-3 PDFs: We obtain the Mellin moments $\langle x^m \rangle_F = \int_{-1}^1 dx x^m F(x)$ via the momentum space approach given by Eq. (7) which yields

$$\langle x^m \rangle_F = \frac{1}{2P \cdot n} \int \frac{d^4 k}{(2\pi)^4} \left(\frac{k_\eta \cdot n}{P \cdot n} \right)^m \text{Tr} [\Phi(k, P) \Gamma_F], \quad (14)$$

with Dirac matrix Γ_F chosen so that F represents f_q or e_q . The results are displayed in Table I. The fact that $\langle x^m \rangle_{e_q}$ decreases rapidly between $m = 0$ and $m = 1$ is a signal of significant strength in $e_q(x)$ near $x = 0$. The analysis [2, 6] which underlies Eq. (2), and the moment properties, begins from the local limit of the bilocal quark field operator in Eq. (1). This emphasizes low x behavior by producing the $\delta(x)$ term which generates the complete 0-th moment $\sigma_\pi/2m_q$. Our DSE-RL approach yields $\langle x^0 \rangle_{e_q}^\pi = 6.45$ which is equivalent to $\sigma_\pi = 0.071$ GeV. This is essentially $M_\pi/2$, an analytic σ_π result that follows from DSE rainbow-ladder truncation [22, 27] combined with the leading order departure of M_π from the chiral limit.

The $\delta(x)$ term in $e_q(x)$ does not contribute to hard scattering processes; it is always $x e_q(x)$ that shows up

in factorized cross sections [14, 28, 29]. It is therefore useful to consider $xe_q(x)$ as the distribution of interest; all of its moments are equivalent to the $\langle x^m \rangle_{xe_q}$ for $m \geq 1$. Our DSE-RL results displayed in Table I indicate that the distribution $xe_q(x)$ has moments $\langle x^m \rangle_{xe_q}^\pi$ that do not monotonically decrease with increasing m ; there is a significant rise from $\langle x^0 \rangle_{xe_q}^\pi = 0.113$ to $\langle x^1 \rangle_{xe_q}^\pi = 0.303$, followed by a slow decrease thereafter. This suggests a distribution that changes sign from negative at small x to positive at large x with at least one node. We find that if $xe_q^\pi(x)$ is parameterized as

$$xe_q^\pi(x) = N(1-x)^b [x^a - 2x^c(1-x)], \quad (15)$$

then an excellent fit to our DSE-RL moments displayed in Table I is obtained with deviation less than 0.5%. We also parameterize the twist-2 pion PDF via [30]

$$f_q^\pi(x) = (1-x)^\beta \sum_{i=0,1,2} c_i x^i, \quad (16)$$

and the DSE-RL moments given in Table I are fit with deviation less than 1%. The resulting parameters are listed in Table II.

We note from Eqs. (2,4) that an exact QCD result for parton momentum is $\langle x^0 \rangle_{xe_q} \equiv \langle x \rangle_{e_q} = \langle x \rangle_{e_q^{\text{mass}}} = m_q/M_\pi$. With our current mass value $m_q = 5.5$ MeV, this would give 0.039, but we obtain 0.113. The difference arises because the DSE-RL truncation approach, based on ladder sums of quark-quark interactions, can not exactly preserve the transformation of the quark-quark correlation under the QCD EOM for the quark field operator that underlies the above. However, our $\langle x^0 \rangle_{xe_q}$ is still much smaller than the next moment $\langle x \rangle_{e_q}^\pi = 0.303$ and that dominates the consequent x -dependence. Moreover, we have verified that $\langle x \rangle_{e_q} \rightarrow 0$ as $m_q \rightarrow 0$, confirming the strong chiral-symmetry constraint on the pion's $e(x)$, consistent with the Gell-Mann–Oakes–Renner relation $m_q \propto M_\pi^2$ near the chiral limit.

$f_q^\pi(x)$	β	c_0	c_1	c_2
	0.704	1.737	-0.3587	0.4464
$xe_q^\pi(x)$	N	a	b	c
	8.493	0.4496	0.7528	0.5512

TABLE II. Fitting parameters for the pion PDFs in Eqs. (15,16).

The considered DSE-RL diagrams in Fig. 1 only constitute a subset of all possible QCD diagrams, e.g., quark–antiquark pair creation and annihilation from the vacuum are ignored. This associates a model scale μ_0 to our approach, at which intrinsic sea quark PDFs are absent, i.e., $f_{\bar{q}}(x; \mu_0) = e_{\bar{q}}(x; \mu_0) = 0$. Given $f_q(-x) = -f_q(x)$ and $e_q(-x) = e_{\bar{q}}(x)$ by definition [1, 2], the obtained PDFs $f_q(x; \mu_0)$ and $xe_q(x; \mu_0)$ are thus only nonzero in the domain $x \in [0, 1]$. The results from fitting the moments are shown in the upper panel of Fig. 2. The model scale

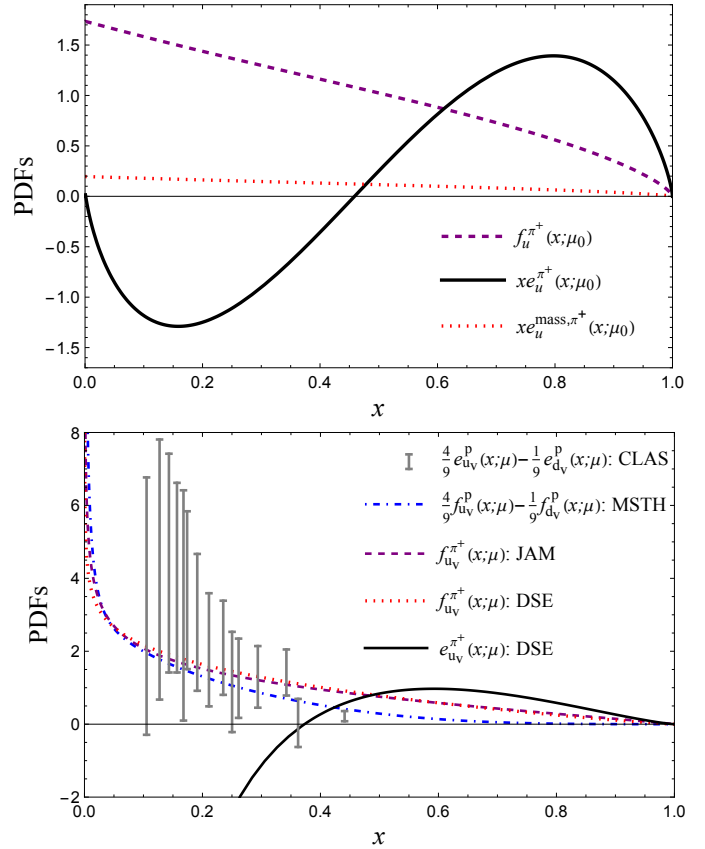


FIG. 2. *Upper Panel:* The pion PDFs at model scale $\mu_0 = 0.63$ GeV. *Lower Panel:* The pion PDFs $f_q(x)$ and $e_q(x)$ at $\mu = 1.3$ GeV with $f_q(x)$ compared to the JAM analysis at NLO [31]. Also shown for comparison are isospin averaged proton PDF data: the $e_q(x)$ CLAS data points at approximately 1 GeV [14], and the MSHT fit of the proton $f_q(x)$ [32].

$\mu_0 \approx 0.63$ GeV is determined after QCD evolution as described below. Noticeably, the $xe_q(x)$ is comparable with $f_q(x)$ in magnitude. Regarding the decomposition in Eq. (2), we estimate for the pion $xe_q^{\text{mass}}(x) \equiv 0.113 f_q(x)$ which saturates the present DSE-RL result $\langle x \rangle_{e_q}^\pi = 0.113$. As a result Fig. 2 shows that the resulting genuine twist-3 contribution $xe_q^{\text{tw3}}(x) = xe_q(x) - xe_q^{\text{mass}}(x)$ is strongly dominant. Moreover, due to the sum rule constraint $\langle x^0 \rangle_{xe_q^{\text{tw3}}} = 0$, the x shape of $xe_q^{\text{tw3}}(x)$ is oscillatory, analogously for the total $xe_q(x)$. The Mellin moments of the estimated pion $e_q^{\text{mass}}(x)$ and the deduced $e_q^{\text{tw3}}(x)$ are displayed in Table I.

The QCD evolution equations of $e_q(x)$ were developed in [6, 33, 34]. At large N_c and in the chiral limit, the moments of the valence $e_q(x)$ obey the simple DGLAP equation similar to $f_q(x)$

$$\langle x^m \rangle_{f_q}(\mu) = L^{Y_n^f/\beta_0} \langle x^m \rangle_{f_q}(\mu_0), \quad n \geq 0 \quad (17)$$

$$\langle x^m \rangle_{e_q}(\mu) = L^{Y_n^e/\beta_0} \langle x^m \rangle_{e_q}(\mu_0), \quad n \geq 2 \quad (18)$$

with $L = \alpha_s(\mu)/\alpha_s(\mu_0)$, $\gamma_n^e = 2N_c \left(S_n - \frac{1}{2(n+1)} - \frac{1}{4} \right)$, $\gamma_n^f =$

$\frac{4}{3} \left(4S_{n+1} - 3 - \frac{2}{(n+1)(n+2)} \right)$, $S_n \equiv \sum_{i=1}^n \frac{1}{i}$ and $\beta_0 = 11 - \frac{2}{3} N_f$. Eq. (18) was found to be a good approximation to the exact one [33]. Here at leading order we take $N_f = 3$ and $\Lambda_{\text{QCD}} = 0.35$ GeV and evolve the PDFs to the scale of $\mu = 1.3$ GeV. The initial scale μ_0 is determined by matching to the JAM global fit result $\langle x \rangle_{f_{q_v}} = 0.268$ [31]. Note the valence combination is defined as $f_{q_v} \equiv f_q - f_{\bar{q}}$, and analogously for e_{q_v} . All other moments of $f_q(x; \mu)$ and $e_q(x; \mu)$ are thus predictions.

The evolved valence PDFs of the pion are shown in the lower panel of Fig. 2. Our $f_{u_v}^{\pi^+}(x; \mu)$ compares well with the JAM analysis at NLO [31], and applying NLO evolution produces only minor modifications. Meanwhile, $e_{u_v}^{\pi^+}(x; \mu)$ exhibits two salient features: (i) its magnitude remains comparable to that of the twist-2 PDF $f_{u_v}^{\pi^+}(x; \mu)$; (ii) the zero-crossing node evident at model scale persists, albeit shifted toward smaller x .

A rainbow-ladder DSE computation of the nucleon's $e(x)$ can be carried out analogously by extending the method developed in this work, albeit at a significantly higher computational cost. In this case, however, the dominance of the genuine twist-3 contribution $e_q^{\text{tw3}}(x)$ in the proton may be less pronounced at hadronic scales, since effective constituent-like quark degrees of freedom become relevant in $x e_q^{\text{mass}}(x) = \frac{\bar{m}_q}{M_h} f(x)$, as chiral symmetry is less constraining than in the pion ². In various model studies, the effective quark mass is found to lie in the range 100–400 MeV [2, 35–38], reflecting the enhancement induced by infrared dynamics at hadronic scales.

Nevertheless, it remains possible that $e_q^{\text{tw3}}(x)$ still contributes substantially. If so, its nodal structure would leave a characteristic imprint—a nonmonotonic hump in $e(x)$ at experimental scales. Such a feature would be absent if $e(x)$ were dominated by the mass term $e_q^{\text{mass}}(x)$ and its evolution pattern. Figure 2 shows the isospin-averaged proton $e_q(x)$ extracted from CLAS [14] together with the central MSHT20nlo fit of $f_q(x)$ [32]. A hump-like feature is compatible with, although not uniquely indicated by, the data, given the sizable experimental uncertainties.

Summary and Outlook: We present the first rainbow-ladder Dyson–Schwinger study of the pion's twist-3 PDF $e_q(x)$. The Mellin moments are computed first and the x distribution is derived from them. The results strongly support the QCD equation-of-motion decomposition of Eq. (2), exhibiting the $\delta(x)$ singularity and a chiral-symmetry suppression of the twist-2 term $e_q^{\text{mass}}(x)$. These findings provide a new picture for the pion $e_q(x)$: the twist-3 quark–gluon piece, rather than the commonly assumed twist-2 term, dominates the distribution. A characteristic feature of the resulting $e(x)$ is a nodal structure and the associated hump. The presently available data, limited by large uncertainties, can neither pin down nor exclude the existence of a hump. Higher-precision measurements are required to clarify this point, and extending measurements to lower x at an Electron–Ion Collider may determine whether the hump evolves into a zero crossing at lower x [3, 4, 39].

Acknowledgement: This work was inspired in part by discussions with the late Professor Fan Wang.

[1] R. L. Jaffe and X.-D. Ji, *Nucl. Phys. B* **375**, 527 (1992).
[2] A. V. Efremov and P. Schweitzer, *JHEP* **08**, 006 (2003), [arXiv:hep-ph/0212044](https://arxiv.org/abs/hep-ph/0212044).
[3] R. Abdul Khalek *et al.*, *Nucl. Phys. A* **1026**, 122447 (2022), [arXiv:2103.05419 \[physics.ins-det\]](https://arxiv.org/abs/2103.05419).
[4] D. P. Anderle *et al.*, *Front. Phys. (Beijing)* **16**, 64701 (2021), [arXiv:2102.09222 \[nucl-ex\]](https://arxiv.org/abs/2102.09222).
[5] R. L. Jaffe and X.-D. Ji, *Phys. Rev. Lett.* **67**, 552 (1991).
[6] A. V. Belitsky and D. Mueller, *Nucl. Phys. B* **503**, 279 (1997), [arXiv:hep-ph/9702354](https://arxiv.org/abs/hep-ph/9702354).
[7] J. P. Ma and G. P. Zhang, *Phys. Lett. B* **811**, 135947 (2020), [arXiv:2003.13920 \[hep-ph\]](https://arxiv.org/abs/2003.13920).
[8] S. Bhattacharya, K. Cichy, M. Constantinou, A. Metz, A. Scapellato, and F. Steffens, *Phys. Rev. D* **102**, 114025 (2020), [arXiv:2006.12347 \[hep-ph\]](https://arxiv.org/abs/2006.12347).
[9] Y. Hatta and Y. Zhao, *Phys. Rev. D* **102**, 034004 (2020), [arXiv:2006.02798 \[hep-ph\]](https://arxiv.org/abs/2006.02798).
[10] M. Wakamatsu and Y. Ohnishi, *Phys. Rev. D* **67**, 114011 (2003), [arXiv:hep-ph/0303007](https://arxiv.org/abs/hep-ph/0303007).

² We emphasize that this discussion is restricted to a model or effective-theory calculation at a hadronic scale. At higher experimental scales, proton's $e_q^{\text{mass}}(x)$ is strongly suppressed by the factor $\frac{m_q}{M_{\text{proton}}}$, so that only $e_q^{\text{tw3}}(x)$ could potentially play a dominant role.

[11] A. Mukherjee, *Phys. Lett. B* **687**, 180 (2010), [arXiv:0912.1446 \[hep-ph\]](https://arxiv.org/abs/0912.1446).
[12] F. Aslan and M. Burkhardt, *Phys. Rev. D* **101**, 016010 (2020), [arXiv:1811.00938 \[nucl-th\]](https://arxiv.org/abs/1811.00938).
[13] A. V. Efremov, K. Goeke, and P. Schweitzer, *Phys. Rev. D* **67**, 114014 (2003), [arXiv:hep-ph/0208124](https://arxiv.org/abs/hep-ph/0208124).
[14] A. Courtois, A. S. Miramontes, H. Avakian, M. Mirazita, and S. Pisano, *Phys. Rev. D* **106**, 014027 (2022), [arXiv:2203.14975 \[hep-ph\]](https://arxiv.org/abs/2203.14975).
[15] R. L. Jaffe, *Nucl. Phys. B* **229**, 205 (1983).
[16] V. Barone, A. Drago, and P. G. Ratcliffe, *Phys. Rept.* **359**, 1 (2002), [arXiv:hep-ph/0104283](https://arxiv.org/abs/hep-ph/0104283).
[17] P. Maris and C. D. Roberts, *Phys. Rev. C* **56**, 3369 (1997), [arXiv:nucl-th/9708029](https://arxiv.org/abs/nucl-th/9708029).
[18] P. Maris and C. D. Roberts, *Int. J. Mod. Phys. E* **12**, 297 (2003), [arXiv:nucl-th/0301049](https://arxiv.org/abs/nucl-th/0301049).
[19] J. C. R. Bloch, *Phys. Rev. D* **66**, 034032 (2002), [arXiv:hep-ph/0202073](https://arxiv.org/abs/hep-ph/0202073).
[20] P. C. Tandy, *Phys. Lett. B* **842**, 137972 (2023), [arXiv:2302.07473 \[hep-ph\]](https://arxiv.org/abs/2302.07473).
[21] K. D. Bednar, I. C. Cloët, and P. C. Tandy, *Phys. Rev. Lett.* **124**, 042002 (2020), [arXiv:1811.12310 \[nucl-th\]](https://arxiv.org/abs/1811.12310).
[22] P. Maris and P. C. Tandy, *Phys. Rev. C* **60**, 055214 (1999), [nucl-th/9905056](https://arxiv.org/abs/nucl-th/9905056).
[23] S.-x. Qin, L. Chang, Y.-x. Liu, C. D. Roberts, and D. J. Wilson, *Phys. Rev. C* **84**, 042202 (2011), [arXiv:1108.0603](https://arxiv.org/abs/1108.0603)

[nucl-th].

- [24] S.-x. Qin, C. D. Roberts, and S. M. Schmidt, *Few Body Syst.* **60**, 26 (2019), arXiv:1902.00026 [nucl-th].
- [25] Z.-Q. Yao, D. Binosi, Z.-F. Cu, and C. D. Roberts, (2024), arXiv:2403.08088 [hep-ph].
- [26] R. D. Tangerman and P. J. Mulders, *Phys. Rev. D* **51**, 3357 (1995), arXiv:hep-ph/9403227.
- [27] V. V. Flambaum, A. Holl, P. Jaikumar, C. D. Roberts, and S. V. Wright, *Few Body Syst.* **38**, 31 (2006), arXiv:nucl-th/0510075.
- [28] P. J. Mulders and R. D. Tangerman, *Nucl. Phys. B* **461**, 197 (1996), [Erratum: Nucl.Phys.B 484, 538–540 (1997)], arXiv:hep-ph/9510301.
- [29] T. B. Hayward *et al.*, *Phys. Rev. Lett.* **126**, 152501 (2021), arXiv:2101.04842 [hep-ex].
- [30] C. Shi, P. Liu, Y.-L. Du, and W. Jia, *Phys. Rev. D* **110**, 094010 (2024), arXiv:2409.05098 [hep-ph].
- [31] P. C. Barry, N. Sato, W. Melnitchouk, and C.-R. Ji, *Phys. Rev. Lett.* **121**, 152001 (2018), arXiv:1804.01965 [hep-ph].
- [32] S. Bailey, T. Cridge, L. A. Harland-Lang, A. D. Martin, and R. S. Thorne, *Eur. Phys. J. C* **81**, 341 (2021), arXiv:2012.04684 [hep-ph].
- [33] Y. Koike and N. Nishiyama, *Phys. Rev. D* **55**, 3068 (1997), arXiv:hep-ph/9609207.
- [34] I. I. Balitsky, V. M. Braun, Y. Koike, and K. Tanaka, *Phys. Rev. Lett.* **77**, 3078 (1996), arXiv:hep-ph/9605439.
- [35] P. Schweitzer, *Phys. Rev. D* **67**, 114010 (2003), arXiv:hep-ph/0303011.
- [36] Y. Ohnishi and M. Wakamatsu, *Phys. Rev. D* **69**, 114002 (2004), arXiv:hep-ph/0312044.
- [37] B. Pasquini and S. Rodini, *Phys. Lett. B* **788**, 414 (2019), arXiv:1806.10932 [hep-ph].
- [38] Z. Zhu, S. Xu, J. Wu, H. Yu, Z. Hu, J. Lan, C. Mondal, X. Zhao, and J. P. Vary (BLFQ), *Phys. Lett. B* **855**, 138829 (2024), arXiv:2404.13720 [hep-ph].
- [39] P. Agostini *et al.* (LHeC, FCC-he Study Group), *J. Phys. G* **48**, 110501 (2021), arXiv:2007.14491 [hep-ex].